DOI 10.5012/bkcs.2010.31.9.2519

Control of Surface Chemistry and Electrochemical Performance of Carbon-coated Silicon Anode Using Silane-based Self-Assembly for Rechargeable Lithium Batteries

Hyun Choi, Cao Cuong Nguyen, and Seung-Wan Song*

Department of Fine Chemical Engineering & Applied Chemistry, Chungnam National University, Daejeon 305-764, Korea
**E-mail: swsong@cnu.ac.kr*
Received May 24, 2010, Accepted July 15, 2010

Silane-based self-assembly was employed for the surface modification of carbon-coated Si electrodes and their surface chemistry and electrochemical performance in battery electrolyte depending on the molecular structure of silanes was studied. IR spectroscopic analyses revealed that siloxane formed from silane-based self-assembly possessed Si-O-Si network on the electrode surface and high surface coverage siloxane induced the formation of a stable solid-electrolyte interphase (SEI) layer that was mainly composed of organic compounds with alkyl and carboxylate metal salt functionalities, and PF-containing inorganic species. Scanning electron microscopy imaging showed that particle cracking were effectively reduced on the carbon-coated Si when having high coverage siloxane and thickened SEI layer, delivering > 1480 mAh/g over 200 cycles with enhanced capacity retention 74% of the maximum discharge capacity, in contrast to a rapid capacity fade with low coverage siloxane.

Key Words: Silane-based self-assembly, Carbon-coated Si, Surface chemistry, Electrochemical performance, SEI layer

Introduction

Silicon (Si)-based materials (e.g., intermetallics, carbon composites) based on alloy reaction with lithium recently have received a particular attention as a next-generation anode materials to replace graphite that is currently used in commercialized lithium-ion batteries, because of larger theoretical specific capacity 3759 mAh/g ($Li_{15}Si_4$) of Si at room temperature than that of graphite.[1-3] A significant crystal structural volume change (>300%) during Li insertion and extraction to/from crystalline Si, which is followed by electrochemical and mechanical disintegration of particles,[4-7] has however been noticed as a major drawback responsible for poor electrochemical performance. Although the volume change could be reduced with amorphous Si, which lowers activation energy barrier and reduces structural strain when reacting with lithium, a capacity decline during electrochemical reaction was inevitable.[6] Many approaches of improvement in the electrochemical performance of Si-based materials have been employed, mostly in a manner which suppresses structural volume changes by modifying bulk materials.[6] Carbon coating on the surface of Si-based materials[8,9] or Si particles embedded into carbon matrix[10-12] seems to be one of the most effective methods. Carbon can enhance electronic conductivity of the electrode and accommodate the volume change. With respect to nanostructure control, much efforts have been ongoing for the development of synthetic strategies by tuning the micro- and nano-structures of Si-based materials releasing the structural stress and enhancing the kinetics.[13-15] Nonetheless, the issues of volume and particle morphology changes seem to be unavoidable, showing the continuous capacity loss with long term Li insertion and extraction.

Recollecting that lithium ion transport should begin to occur at the electrode/electrolyte interface, structural volume change followed by particle cracking event will accompany the change in active surface area that should be correlated to the surface chemistry of Si-based materials. Consensus regarding the surface chemistry and its relationship with performance are yet to be reached. We found that the Si reacted with lithium salt-derived species more actively than carbonate-based organic solvents in the conventional electrolyte,[16] which was somewhat different interfacial process from that of lithiated graphite that formed a stable solid-electrolyte interphase (SEI) layer composed of primarily organic compounds mostly during initial cycling.[17] It was claimed that the surface of Si needed to be protected from lithium salt of electrolyte.[16]

Organoalkoxysilane is of our particular interest as a surface modifying agent to Si, since the organoalkoxysilane can form the Si-O-Si molecular linkages with the surface silanol groups of Si.[16,18,19] The Si-O-Si molecular cross-linking for the formation of siloxane occurs *via* axial self-assembly following intermolecular condensation; —Si-OH + $Si(R)_{4-x}(OR)_x$ → —Si-O-$Si(R)_{4-x}(OR)_{x-1}$ + ROH (R = alkyl group).[20] The presence of trace water assists the hydrolysis of silanes and equatorial polycondensation on neighboring silane molecules, forming three dimensional (3D) self-assembled siloxane network.

Systematic studies of thin-film model electrode that possesses enlarged surface to volume ratio can provide a clearer insight into self-assembly phenomena, electrode/electrolyte interfacial reaction and electrochemical processes of material, and permit convenient analyses of the SEI composition without complications from carbon and binder additives that are necessary in bulk materials.[16,21-24] Polymeric binder often gives interfering signals in IR spectroscopic data, which obstructs distinguishing newly formed surface species from the binder. Thin-films prepared with pulsed laser deposition (PLD), which generally possess a strong physical interfacial adherence to electronically conductive substrate, allow the observation of material's intrinsic surface structure and reaction, and inhibit a peel-off

event of the film during extended cycling in lithium cells. For the surface characterization, we focus on ex-situ IR measurement with attenuated total reflection (ATR) geometry that is very sensitive to surface species and provides direct information on the functional groups of surface molecules.[22-26]

Here we report a surface modification approach to stabilize surface structure and cycling performance of carbon-coated Si thin-film electrode. Surface modification by self-assembly of organoalkoxysilanes with different number of organoalkoxy group and SEI layer formation resulting from electrode/electrolyte interfacial reactions were determined using ex-situ IR spectroscopy with attenuated total reflection (ATR) geometry. Interfacial reaction behavior-performance relationship is discussed.

Experimental

Films of Si were first prepared on stainless steel substrates with PLD at 200 ^{o}C with 20 min deposition in 5 mtorr of Ar. Deposition utilized a KrF eximer laser with an energy density of 3 - 4 mJ/cm^2 at 10 Hz impinging on a target (ICM Engineering). Film thickness and morphology were evaluated by a field emission scanning electron microscope (FE SEM, Jeol JSM-7000F) at 5 kV. The observed film thickness of the as-prepared Si film was 47 - 74 nm. The 10 nm thick carbon film was coated over the film of Si (denoted as C-Si hereafter) by precision etching coating system (PECS, Gatan Inc. 682 PECS™) with ion beam current of 200 - 250 μA. Elemental distribution of Si and C over the film was obtained using electron mapping of SEM. The film structure was identified by X-ray diffraction using an X-ray diffractometer (Rigaku D/MAX-2200) with Ni filtered Cu Kα radiation at 40 kV and 40 mA, and a scan rate of 1.5^{o}/min from 20 to 70^{o} 2θ with 0.02^{o} steps. Further structural characterization of Si and coated carbon was carried out using Raman spectroscopy. Raman spectral measurement was conducted for 120 - 240 s using a closed prototype Raman cell, where the film surface was placed below the glass window in the glove box, then, the cell was tightly sealed. Raman spectra were recorded using a Raman microscope (Tokyo instrument Co., Nanofinder 30) at ambient conditions, using the 632 nm line of a He-Ne laser at 1 mW. Backscattering optics geometry with double-notch filter and a standard charge-coupled device (CCD) detector were used to collect, process, and analyze the Raman signal. The size of the laser beam at the sample was less than 200 nm.

In order to examine self-assembly of silanes on the C-Si, several identical as-prepared C-Si film electrodes were immersed in the jars filled with approximately 5 mL of 1-(trimethylsilyloxy)-1,3-butadiene (CH_2=CHCH=CHOSi(CH_3)$_3$, Aldrich), methyltrimethoxysilane ($CH_3Si(OCH_3)_3$, Aldrich), and tris(2-methoxyethoxy)vinylsilane (CH_2=CHSi((OCH_2CH_2)$_2OCH_3$)$_3$, Aldrich) for 3 hrs, respectively. Then, the films were separated from the silane solution and thoroughly washed with dimethyl carbonate (DMC, Techno Semichem) for 30 s and dried in the glove box at room temperature. For the film immersed in tris (2-methoxyethoxy)(vinyl)silane, longer washing of 3 hours with DMC was conducted for further removal of silane moiety. Surface identification for the C-Si obtained after self-assembly reaction with different silanes was carried out with ATR FTIR spectroscopy, using IR spectrometer (Bruker optics IFS66V/S) equipped with a mercury-cadmium-telluride (MCT) detector. Prior to the measurements the films were directly mounted on the closed single reflection ATR unit with a Ge optic in the Ar-filled glove box, then, the FTIR spectra were acquired. There was no moment of atmospheric contamination. Spectral resolution was of 4 cm^{-1} and a total of 512 scans were co-added.

Electrochemical cells, containing C-Si film electrode as a working electrode with Li reference and counter electrodes, have been used for electrochemical evaluation. The lithium cells with the film electrode were cycled at a constant current of 35 μA/cm^2 between 0.1 and 1.5 V *vs.* Li/Li$^+$ at room temperature, in the electrolyte of 1 M $LiPF_6$/ethylene carbonate (EC): diethyl carbonate (DEC) with 1:1 volume ratio (Techno Semichem) without or with 5 wt % silanes as additives, using a multichannel cycler (Wonatech). The cycled films were separated from the lithium cells and thoroughly washed with DMC and dried in the glove box at room temperature for *ex-situ* characterization. All self-assembly reactions and electrochemical experiments with lithium cells were conducted in the Ar-filled glove box with the water and oxygen contents of about 1 ppm. Surface chemistry of the film electrodes obtained after cycling was studied using ex-situ ATR FTIR spectroscopy. Changes in the film morphology of C-Si film electrodes before and after cycling were characterized by *ex-situ* FESEM and Raman spectroscopy.

Results and Discussion

Characterization of carbon-coated Si electrode. Surface morphology of the as-prepared C-Si appears smooth in Fig. 1a. Raman spectrum of the film in Fig. 1b exhibits a sharp band at 516 cm^{-1}, characteristic of crystalline Si,[27] and equally intense and broad bands at 141, 320 and 472 cm^{-1} that are due to amorphous Si.[28,29] Although the as-prepared Si only film was crystalline, discernable from the XRD pattern (not shown), after carbon-coating the film became partly disordered or amorphous. Also shown is a broad band at around 1500 cm^{-1} corresponding to graphite-like sp^2 carbon (G-band),[30,31] which indicates that graphite-like carbon is dominant in the coated carbon layer. Fig. 1c and d exhibit elemental distribution of Si and C atoms in the film. Homogeneous but scattered distribution of C atoms is indicative of a porous feature of the carbon layer, as often occurs on carbon-coated Si and Si-carbon composite bulk materials. Note that bare Si of the film could be exposed to electrolyte.

Surface modification of carbon-coated Si electrode. Formation of siloxane between the as-prepared C-Si film and silane was monitored by ATR FTIR spectroscopy. Figure 2 shows IR spectra for the surface of the C-Si film obtained after immersing in three different silanes (Fig. 2a-c) followed by DMC washing. The surface layer of the as-prepared Si before carbon coating showed the IR signature of silanol (-Si-OH) group at 850 - 830 cm^{-1} [16,18] (not shown). For the film surface immersed in 1-(trimethylsilyloxy)-1,3-butadiene, Fig. 2a' exhibits prominent peaks at 1103 and 1024 cm^{-1} due to asymmetric stretching modes of Si-O-Si functionality.[31-33] Sharp peaks at 1268 and 814 cm^{-1}

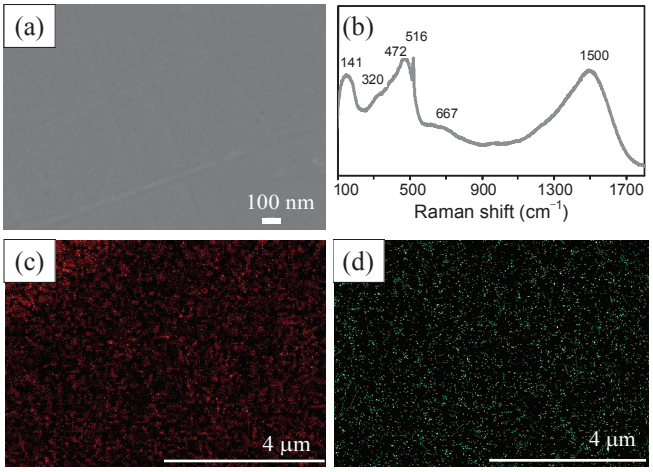

Figure 1. SEM image of surface morphology (a) and Raman spectrum (b) for the as-prepared carbon-coated Si film, and electron mapping results of (c) Si (red) and (d) C (green) elements.

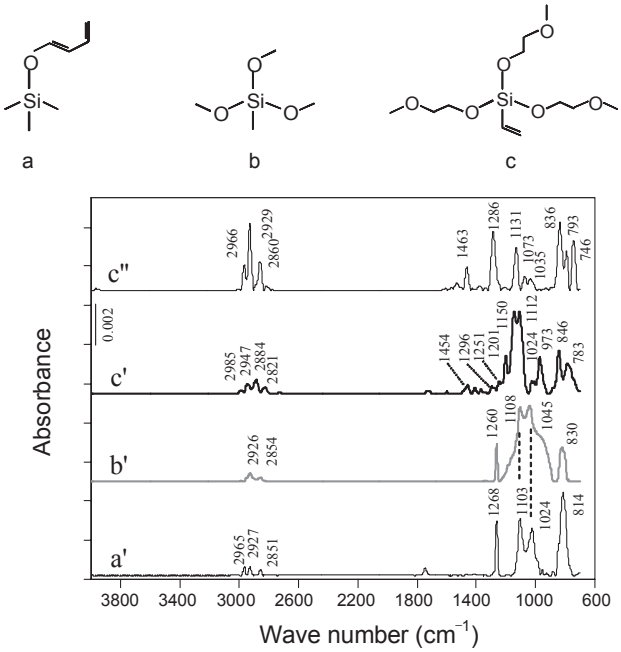

Figure 2. Molecular structure of 1-(trimethylsilyloxy)-1,3-butadiene (a), methyltrimethoxysilane (b) and tris(2-methoxyethoxy)vinylsilane (c). IR spectra for the as-prepared Si film and the carbon-coated Si obtained after immersing in the (a') 1-(trimethylsilyloxy)-1,3-butadiene, (b') methyltrimethoxysilane and (c') tris(2-methoxyethoxy) vinylsilane followed by DMC washing for 30s, (c'') washing for 3 hrs and drying.

are attributed to deformation of -CH_3 from Si-CH_3 group and stretching mode of Si-C together with -CH_3 rocking, respectively.[31,32] Signature of silanol group was no longer clearly distinguished and must be used up for self-assembly. This evidences that siloxane formed at the surface of C-Si by self-assembly condensation between surface silanol group and one alkoxy group from this silane, resulting in the formation axial 1D Si-O-Si molecular linkages. Three methyl groups of 1-(trimethylsilyloxy)-1,3-butadiene remains perhaps available for further reaction with electrolyte components or physical interaction with electrolyte or SEI component. Tiny peaks at 2965 - 2851 cm^{-1} due to -CH_3 group support this assignment.

Similar spectral feature was observed for the film immersed in methyltrimethoxysilane in Fig. 2b', except that the peaks at 1108 and 1045 cm^{-1} due to Si-O-Si group of siloxane became relatively stronger than that of Si-C functionality observed near 830 cm^{-1}. Since three methoxy groups in methyltrimethoxysilane could be consumed for the formation of Si-O-Si linkages, one axial Si-O-Si bond from each silane to the silanol of Si surface can be produced, whereas two other remaining alkoxy groups are utilized for equatorial condensation between silanes leading to 3D Si-O-Si network. In this case the siloxane chain of Si-O-Si functionality should be longer and branched compared to the siloxane with only axial linkage from single alkoxy-containing silane, thereby, enhances the peaks absorbance and makes the peaks broader. Surface coverage with 3D siloxane network however may be limited because of physical dimension by the presence of porous carbon layer.

With tris(2-methoxyethoxy)vinylsilane the film surface in Fig. 2c', obtained after DMC washing for 30s, shows the peaks for both asymmetric Si-O-C stretching of silane and Si-O-Si functionality of siloxane at 1150, 1112 and 1024 cm^{-1}, respectively,[31-33] referred to the original spectrum of tris(2-methoxyethoxy)vinylsilane.[33] This indicates that some alkoxy group of silane is utilized for the formation of siloxane, whereas others remained as attached to the siloxane. Other peaks at 2985 - 2821 cm^{-1} for -CH_2- and CH_3 stretching and their deformation at 1454 - 1403 cm^{-1}, and also -O-C group at 1201 cm^{-1}, symmetric Si-O-C stretching at 973 and 846 cm^{-1} and 783 cm^{-1} for -CH_2-rocking of oxaethylene chains -$(OCH_2CH_2)_2$-OCH_3,[31,32] respectively, and -CH_2 wagging of vinyl group at 973 cm^{-1} support the presence of silane moiety. In general, the condensation reactions become sluggish with greater bulk alkoxy group because of steric hindrance. In Fig. 2c'', further DMC washing for 3hrs resulted in a disappearance of the peaks corresponding to the silane moiety. However several sharp peaks, attributed to oxaethylene -(OCH_2CH_2)-OCH_3 of silane, are still discernable. Eventually the film surface became decorated with the organic silane moiety, like "artificial" surface layer. This enlarges surface coverage of siloxane at most among the silanes used in this work. The resultant data ensures that in the presence silane, self-assembly of siloxane occurs on the surface of the C-Si.

Cycling behavior of surface modified electrode. Cycling behavior of the C-Si in the presence of silanes was evaluated using constant current cycling at 35 μA/cm^2 (~ 1C for $Li_{15}Si_4$) in the voltage region of 0.1 - 1.5 V *vs*. Li/Li$^+$, where structural stress by amorphization-crystallization of Si was avoided.[3] The capacities of a lithium cell with C-Si were obtained by calculation based on the film thickness of Si film and coated carbon layer, electrode area (0.283 cm^2) and crystallographic densities of Si (2.33 g/cm^3) and carbon (1.4 g/cm^3). Some errors (*ca*. 10 - 20%) in capacity values can come from film thickness evaluation and the use of theoretical crystallographic densities of Si and carbon. The capacity *vs*. voltage plots are shown in Fig. 3a-d. Differential capacity plots (Fig. 3a'-d'), obtained from the voltage profiles in Fig. 3a-d, show a better peak resolution of the Si reaction with lithium. In 1 M $LiPF_6$/EC:DEC electrolyte in the absence of silane, the first charge (cathodic) curve (Fig.

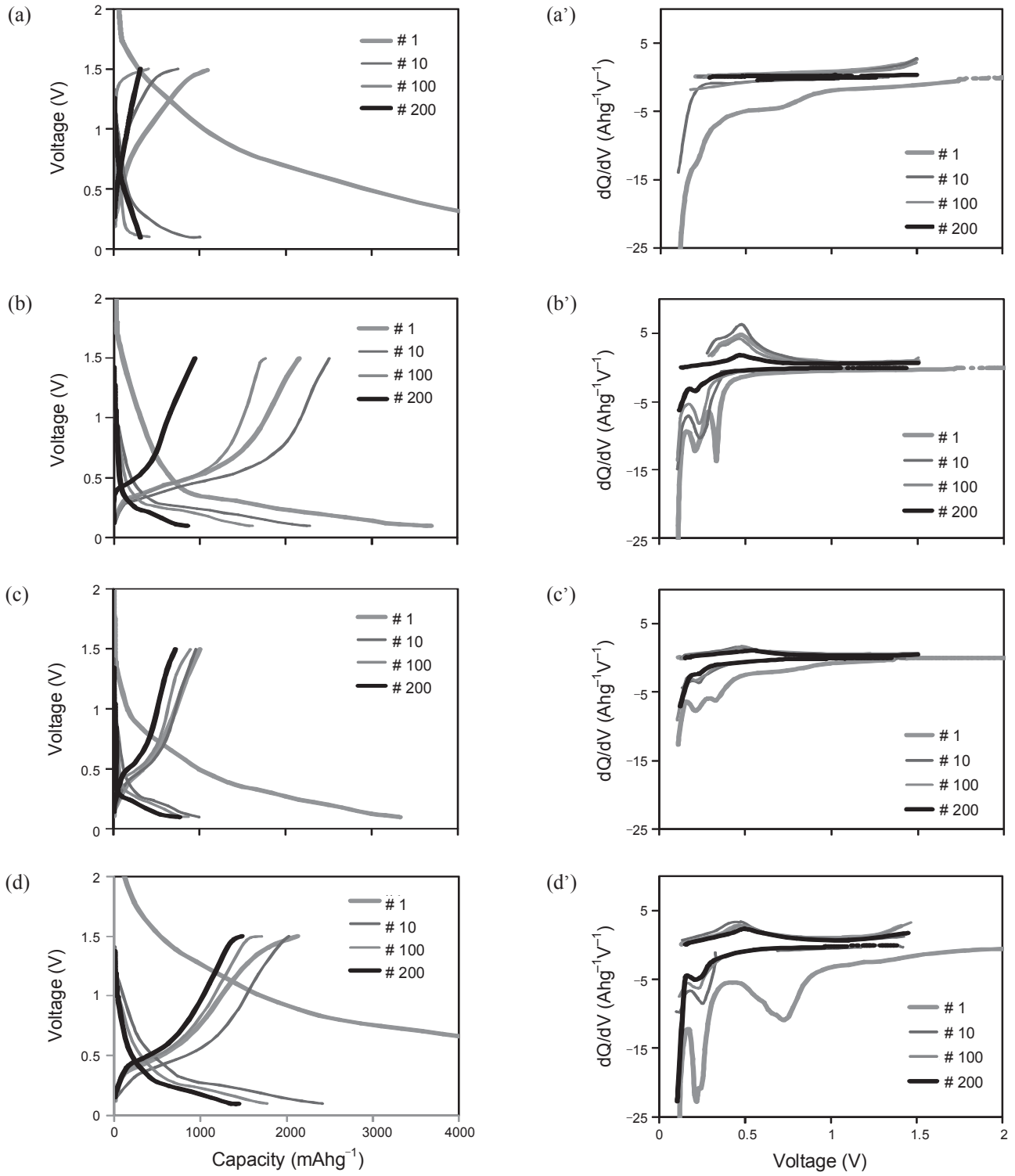

Figure 3. Capacity *vs.* voltage plots of the lithium cells with carbon-coated Si electrode in 1 M $LiPF_6$/EC:DEC without silane (a), and with (b) 1-(trimethylsilyloxy)-1,3-butadiene, (c) methyltrimethoxysilane and (d) tris(2-methoxyethoxy)vinylsilane between 0.1 and 1.5 V *vs.* Li/Li^+, and their differential capacity (dQ/dV) plots (a')-(d').

3a') showed a broad and significant cathodic contribution from 2.0 to 0.5 V, which has been attributed to the reduction of the electrolyte components of EC (calculated reduction potential 1.46 V *vs.* Li/Li^+), and DEC (calculated reduction potential 1.33 V),[34,35] and decomposed and hydrolyzed species of $LiPF_6$ salt.[35] Reduction of electrolyte components on the C-Si seems to be severe. The salt of $LiPF_6$ is known to be in the equilibrium as $LiPF_6 \leftrightarrows PF_5 + LiF$. The presence of a trace of water in the electrolyte produces PF_3O; $PF_5 + H_2O \rightarrow PF_3O + 2HF$.[36] Since both gaseous PF_5 and PF_3O are strong Lewis acids, they can readily react with the C-Si that possesses a plenty of electrons to donate in our operating voltage region, forming M-PF_5 or

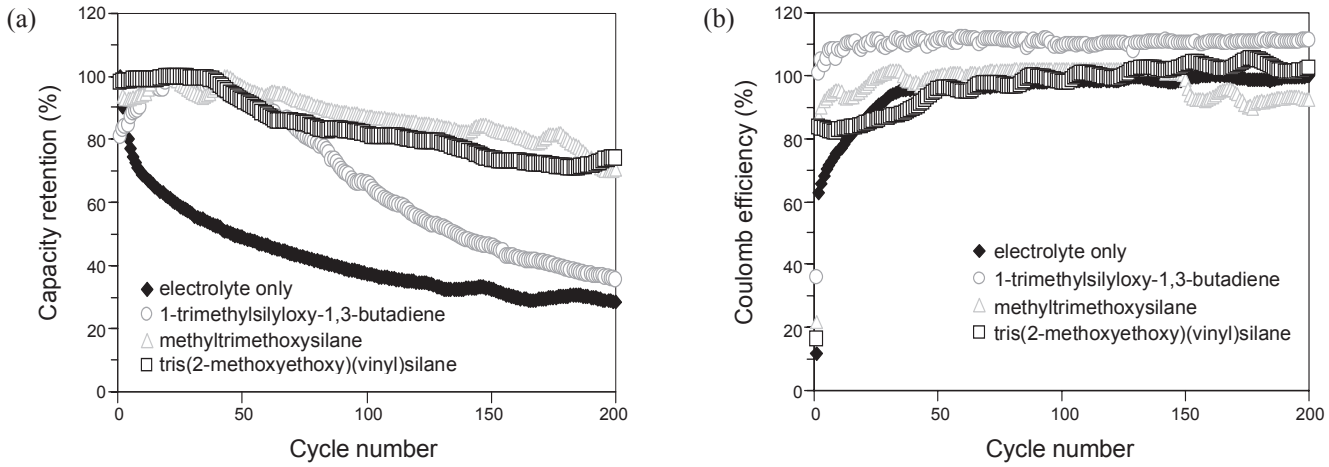

Figure 4. Capacity retention (a) and Coulomb efficiency (b) of the lithium cells with carbon-coated Si electrode without and with silanes, as a function of cycle number.

M-PF_3O (M = Li/Si) type precipitates followed by participating in the further electrochemical reduction. The HF, the hydrolysis product of PF_5, is predicted to etch and modify the surface morphology of the C-Si. At the voltage region below 1.0 V, further reduction of surface species that were formed at higher voltages took place showing still large cathodic contribution, which indicates the reformation of surface composition. This process is followed by the large capacity shoulder at approximately 0.25 V, corresponding to main Li insertion into amorphous Si, forming $Li_{3.25}Si$ and/or the amorphization of Si, consistent with earlier literatures.[1,3,37] After the first charge process, all the peaks disappeared. Such irreversible capacity loss continuously occurred over 200 cycles, resulting in very low capacity retention 28% in Fig. 3a-a' and Fig. 4a, and poor efficiencies ((discharge capacity/charge capacity) × 100) as displayed in Fig. 4b. In addition to electrolyte reduction, irreversibility in Li insertion and extraction should be responsible for this continued irreversible capacity loss.

With 1-(trimethylsilyloxy)-1,3-butadiene, Fig. 3b-b', the C-Si shows sharper peaks for Li insertion and extraction, in contrast to the film without silane (Fig. 3a-a'). The film maintained structural resolution till the 100th cycle despite a large capacity loss to 66% of maximum capacity. In the first charge curve, Fig. 3b', cathodic contribution down to 0.4 V is little, in contrary to the film without silane (Fig. 3a'). This reveals that reductive electrolyte decomposition is dramatically reduced. The cathodic peaks between 0.1 and 0.3 V are due to Li insertion for the phase change to $Li_{12}Si_7$ to $Li_{3.25}Si$.[37] On the subsequent discharge process, the anodic peaks at 0.3 - 0.5 V are due to Li extraction toward the regeneration of Si. Self-assembled siloxane from 1-(trimethylsilyloxy)-1,3-butadiene was effective in suppressing electrolyte decomposition and increasing the reversibility in the early cycles. Nonetheless, after ~100 cycles the film exhibited a disappearance of all the peaks with the occurrence of a drastic capacity decline to 36% of maximum discharge capacity over 200 cycles (Fig. 4a), with poor efficiencies >100% in Fig. 4b. Although silanols at the surface of bare Si and 1-(trimethylsilyloxy)-1,3-butadiene formed self-assembled siloxane, the axial Si-O-Si linkages only and low surface coverage must be insufficient to endure the changes in structural volume and particle morphology during repeated Li insertion and extraction. Since the low surface coverage of siloxane allows direct electrode-electrolyte interfacial contact, during discharge the electron transfer from electrode to electrolyte followed by reductive electrolyte decomposition can provide additional discharge capacity to that by delithiation process. This is related to the efficiencies higher than 100%. Silane with a single alkoxy group appears to offer only limited effect on the performance.

In Fig. 3c-c', the C-Si with methyltrimethoxysilane that comprises three methoxy groups exhibited somewhat improved cycling ability compared to single alkoxy-containing silane. The film electrode shows 71% capacity retention of the maximum discharge capacity at the 200 th cycle but capacities lower than 1000 mAh/g, in Fig. 4a. The 3D siloxane network confers improved surface protection of the C-Si and capacity retention. However, efficiencies in Fig. 4b were reduced to 92% after 150 th cycle. Even though cycling performance was much improved when having 3D siloxane, in contrast to 1D or absence of siloxane, the ability of surface protection by siloxane in this case appeared to be limited.

For the tris(2-methoxyethoxy)vinylsilane the C-Si showed a remarkably improved capacity retention with enhanced capacity values. In Fig. 3d-d', except the first cycle, the prominent structural resolution is remained throughout the 200th cycle. In the first charge process, Fig. 3d', significant cathodic capacity between 2.0 and 0.5 V is observed, which is not observed in the following cycles. This is related to the SEI formation by reductive electrolyte decomposition. The -(CH=CH_2) vinyl functionality of tris(2-methoxyethoxy)vinylsilane is known to undergo cathodic electro-polymerization around 0.8 V at the surface of electrode.[38,39] The polymerization process could increase additionally the cathodic capacity, despite its low concentration level 5 wt %. Large capacities of 1480 - 2130 mAh/g and preserved capacity retention of 74% over 200 cycles in Fig. 4a should be due to the effective surface protection of the C-Si with high surface coverage siloxane and silane moiety first and then additional passivation with the SEI components.

Figure 4 compares the impact of the type of silane on the cycling performance of the C-Si. Overall, in the presence of silanes discharge capacities and capacity retention were improved, in contrast to a rapid capacity decline after the first cycle in the absence of silane. However, even in the presence of self-assembled siloxane, the initial irreversibility due to the reductive decomposition of electrolyte components forming the SEI layer (Fig. 3b'-d') was observed in common. Considering that greater cycling performance was obtained when using the silane that contains three alkoxy functionalities with relatively longer organic chain (Fig. 2c-c'), the surface coverage of self-assembled siloxane network was determined to be the key factor affecting cycling performance of the C-Si.

Characterization of the SEI layer using IR spectroscopy. Surface chemistry of the C-Si in the silane-containing electrolyte was investigated by characterizing the surface species produced on the film electrode surface due to cycling, using ex-situ ATR FTIR spectroscopy. Figure 5 shows IR spectra for the C-Si surface obtained after cycling without and with silanes. Tentative assignments to the vibrational modes are made as the following. Note that when the electrodes were rinsed in DMC prior to IR analysis, soluble surface species could be washed off.

After cycling in the electrolyte without silane, Fig. 5a-a', the C-Si surface shows strong IR features below 900 cm^{-1}, mostly originated from inorganic compounds. Predominant peaks below 890 cm^{-1} are assigned to stretching modes of P-F probably in different molecular bonding nature. The $LiPF_6$-derived compounds, PF_5 and PF_3O [16,36] must be involved in the formation of PF-containing species and as a consequence LiF salt may form automatically as described above. However LiF is not detectable in the mid-IR region used in this work. The data indicate that PF-containing species (e.g., M — P_nF_m (M = Li/Si)) are the major surface species**.** This may indirectly indicate that LiF also forms on the electrode surface. The film also shows the trace of C=O for alkyl carbonate metal salt R-OCO_2^- M^{n+} (R= alkyl, M = Li/Si) and/or R-CO_2^- M^{n+} carboxylate metal salt in the region of 1720 - 1550 cm^{-1} and CH_3-CH_2- alkyl group at 2960 - 2800 cm^{-1}, related to the reduction of organic carbonate solvents.[16,17,22-24,31,32,40-42]

With 1-(trimethylsilyloxy)-1,3-butadiene, Fig. 5b-b', the C-Si surface also shows strong IR features below 900 cm^{-1}, where they are mostly due to PF-containing inorganic compounds. No signature of Si-O-Si functionality from siloxane between 1000 and 1130 cm^{-1} is observed. Reminding that the film with 1-(trimethylsilyloxy)-1,3-butadiene had only axial 1D Si-O-Si linkages and exhibited a rapid capacity decline around the 100th cycle (Fig. 3b-b' and 4), self-assembled siloxane may be collapsed at some point in the middle of cycling. Then, at the 200th cycle the film surface is eventually covered by only PF-containing species, like the surface composition obtained after cycling without silane.

On the C-Si surface after cycling with methyltrimethoxysilane, Fig. 5c-c', IR signatures from P-F containing species are mainly observed. Trace of some organic species is visible but in a very low absorbance. Tiny peaks due to alkyl and C=O group of R-CO_2^- M^{n+} carboxylate salts are shown near 1544 cm^{-1}.[16,17,22-24,31,32] Newly appeared tiny peaks at 1307, 1153, 1016, 833 cm^{-1} are ascribed to stretching modes of P=O, P-O-C and P-F group from -O=PF-OR organic phosphorus-fluorine compounds.[31,32,43] They are partly overlapped with the peaks at 1108 and ~1045 cm^{-1} characteristic of siloxane chain,[16,31,32] in Fig. 2b'. Note that for the C-Si comprising no siloxane or low surface coverage siloxane, inferior cycling performance (Fig. 3a-b) and mainly PF-containing surface species (Fig. 5a-b) were observed. In this context, the presence of mainly PF-containing surface species indicates the limitation in surface protection of siloxane. This is why capacity retention relatively improved but low capacities and a decrease in efficiency in the late stage of cycling (Fig. 4).

On the other hand, cycling the C-Si with tris(2-methoxyethoxy)vinylsilane resulted in a very different spectral feature from those cycled with other silanes. In Fig. 5d-d', signatures from CH_3CH_2- alkyl group at 2960 - 2850 cm^{-1} are significantly strong, indicating that organic compounds including alkyl functionality are one of the major SEI components. Lower absor-

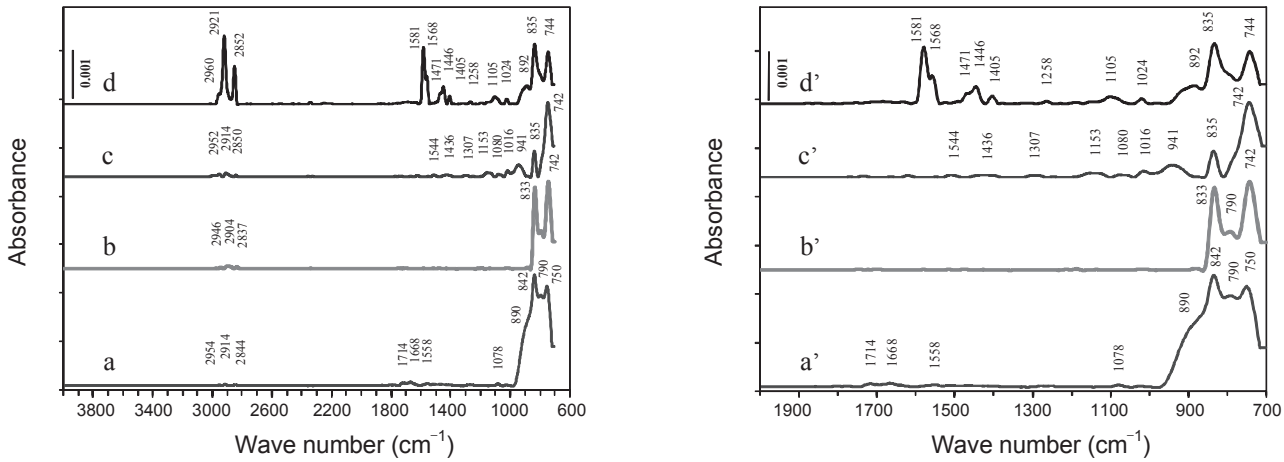

Figure 5. IR spectra for carbon-coated Si electrode obtained after cycling (a) without silane, and with (b) 1-(trimethylsilyloxy)-1,3-butadiene, (c) methyltrimethoxysilane and (d) tris(2-methoxyethoxy)vinylsilane between 0.1 and 1.5 V *vs*. Li/Li^+, followed by DMC washing and drying, and (a')-(d') their magnifications.

bance peaks near 1471 - 1405 cm^{-1} come from the deformation of alkyl group. Remind that after self-assembly the film showed the alkyl and other functionallities from silane moiety (Fig. 2c'-c''). The presence of silane moiety and/or polymerization of vinyl group of silane contributes to enhancement of absorbance of alkyl group. Another strong peaks at 1581 and 1568 cm^{-1} are assigned to C=O carbonyl group of R-CO_2^- M^{n+} (R = alkyl, M=Li/Si) carboxylate metal salt functionalities in different chemical bonding nature of -CO_2^-.[31,32] Lower absorbance peaks near 1260 - 1020 cm^{-1} attributed to finger prints of C=O and C-O stretching of carboxylate support this assignment.[31,32] Alkyl and carboxylate metal salt groups are included to the decomposition products of carbonate-based organic solvents (EC, DEC). Intense features from organic phosphorus-fluorine compounds and other P-F containing inorganic species are also observed in the region of 1260 - 835 cm^{-1}.[31,32,43] Overlapping of a number of peaks in the region of 900 - 800 cm^{-1} including P-F stretchings enhances the peak near 835 cm^{-1}. For the peak weakening of the funtionalities for siloxane and silane moiety, the SEI layer components must be in a higher concentration level than them, thereby, their peaks are hidden under other intense peaks from SEI components. Effective surface passivation of the electrode by those accumulated SEI species is of benefit in protecting the film surface from direct interfacial reaction with electrolyte, improving capacity retention as observed in Fig. 3d-d' and 4.

The IR analysis results indicate that the SEI layer formed by cycling with tris(2-methoxyethoxy)(vinyl)silane is composed of mainly organic compounds with the functionalities of alkyl, and carboxylate metal salt, and inorganic compounds including organic phosphorus compounds and other P-F containing species. Self-assembled siloxane and the presence of silane moieties induced the formation of a plenty of the SEI components. Since more stable capacity retention of the C-Si was attained when large amounted organic and PF-containing inorganic SEI compounds were produced, the efficient protection of the C-Si surface with high coverage siloxane network is believed to be the origin of improved electrochemical performance.

Morphology changes with cycling. Morphology change in the C-Si due to cycling was examined using ex-situ SEM. Figure 6a-d show the surface SEM images of the C-Si after 200 cycles without and with silanes. After cycling without silane, Fig. 6a, film cracking was severe and film appeared brittle, as often observed on Si-based alloy materials.[4-6] Film surface obtained after cycling with 1-(trimethylsilyloxy)-1,3-butadiene, Fig. 6b, was quite a coarse and porous. The particles were somewhat separated from each other. Drastic performance decline during cycling (Fig. 3b-b' and 4) is correlated to this severe morphology change, supporting that surface protection was inferior (Fig. 5b-b'). With methyltrimethoxysilane, Fig. 6c, overall film surface was relatively smooth but film had cracks, although the film appeared still dense. By contrast, with tris(2-methoxyethoxy)vinylsilane the film surface, Fig. 6d, remained smooth, with several round particles in the diameter of 70 - 330 nm. Neither film cracking nor particle aggregation was observed. Surface modification with high coverage siloxane network was effective in reducing the mechanical disintegration of particles. This demonstrates that film morphology change of the C-Si with cycling is strongly dependent on surface chemistry.

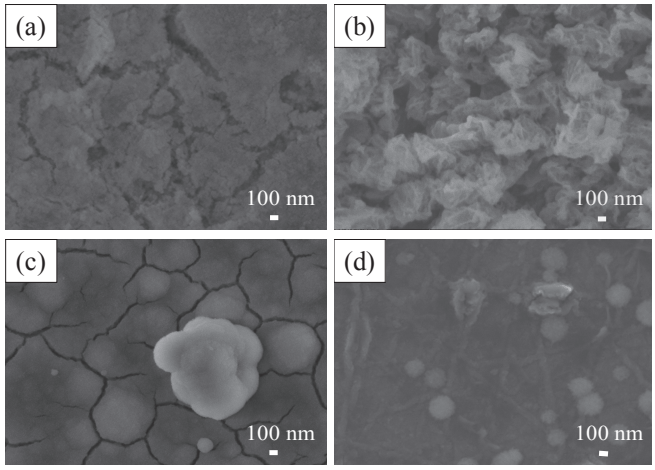

Figure 6. SEM images of surface morphology for carbon-coated Si electrode obtained after cycling (a) without silane, and with (b) 1-(trimethylsilyloxy)-1,3-butadiene, (c) methyltrimethoxysilane and (d) tris(2-methoxyethoxy)vinylsilane.

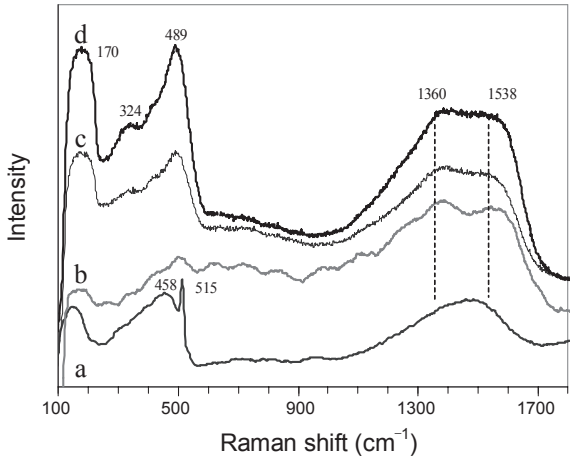

Figure 7. Raman spectra for carbon-coated Si electrode obtained after cycling (a) without silane and with (b) 1-(trimethylsilyloxy)-1,3-butadiene, (c) methyltrimethoxysilane and (d) tris(2-methoxyethoxy) vinylsilane.

Raman spectroscopy provided supportive information on changes in film morphology and surface composition on the C-Si. Figure 7 shows Raman spectra of the C-Si obtained after 200 cycles without and with silanes. After cycling without silane, the spectral feature (Fig. 7a) of the film resembles the as-prepared film (Fig. 1b). However, with cycling in the presence of silanes the films showed spectral changes. In Fig. 7b-d, the sharp band at 515 cm^{-1} from crystalline Si [27] disappeared but a new band at 489 cm^{-1} characteristic of amorphous Si appeared instead.[28,29] All crystalline Si must be converted to amorphous Si, consistent with previous report.[16] Newly noticed was the appearance of a strong and broad band near 1360 cm^{-1} due to diamond-like sp^3 carbon (D-band).[30,31] Diamond-like carbon is associated with the presence of organic SEI compounds and siloxane, which include sp^3-coordinated carbon. Or graphite-

like carbon (G-band), which was originally of the as-prepared C-Si, could be partly converted to diamond-like one by cycling.

Conclusions

The surface of carbon-coated Si was modified by self-assembly of siloxane network using monoalkoxy-, trialkoxy- and trialkoxy-silane with long oxaethylene chain as additives for stabilizing cycling performance of carbon-coated Si in the electrolyte of 1M $LiPF_6$/EC:DEC. The use of longer chain trialkoxysilane was effective in building up 3D siloxane network with high surface coverage and suppressing direct electrode/electrolyte interfacial reaction after the early stage of cycling, which increased the reversibility in cycling. Self-assembled siloxane network led to the formation of a stable SEI layer primarily consisting of organic compounds and PF-containing inorganic species. Simultaneously particle cracking event was efficiently reduced, and capacity value and retention were dramatically improved. Since cycling performance, surface composition and particle morphology change were strongly dependent on the surface coverage of siloxane network, the selection of an appropriate silane is of great impact on the performance control of carbon-coated Si. The data suggest that the control of surface chemistry is necessary to attain high performance lithium-ion batteries employing Si-based alloy anode materials.

Acknowledgments. This work was supported partly by Mid-career Researcher Program (No.2009-0083817) and partly Basic Science Research Program (NRF-2009-0070922) through the National Research Foundation of Korea funded by the Ministry of Education, Science and Technology.

References

1. Netz, A.; Huggins, R. A.; Weppner, W. *J. Power Sources* **2003**, *119-121*, 95.
2. Hatchard, T. D.; Dahn, J. R. *J. Electrochem. Soc.* **2004**, *151*, A838.
3. Obrovac, M. N.; Christensen, L. *Electrochem. Solid-State Lett.* **2004**, *7*, A93.
4. Beaulieu, L. Y.; Eberman, K. W.; Turner, R. L.; Krause, L. J.; Dahn, J. R. *Electrochem. Solid-State Lett*. **2001**, *4*, A137.
5. Lee, S. J.; Lee, J. K.; Chung, S. H.; Lee, H. Y.; Lee, S. M.; Baik, H. K. *J. Power Sources* **2001**, *97-98*, 191.
6. Kasavajjula, U.; Wang, C.; Appleby, A. J. *J. Power Sources* **2007**, *163*, 1003.
7. Obrovac, M. N.; Krause, L. J. *J. Electrochem. Soc*. **2007**, *154*, A103.
8. Dimov, N.; Kugino, S.; Yoshio, M. *Electrochim. Acta* **2003**, *48*, 1579.
9. Ng, S.-H.; Wang, J.; Wexler, D.; Konstantinov, K.; Guo, Z.-P.; Liu, H.-K. *Angew. Chem. Int. Ed*. **2006**, *45*, 6896.
10. Niu, J.; Lee, J. Y. *Electrochem. Solid-State Lett*. **2002**, *5*, A107.
11. Yang, J.; Wang, B. F.; Wang, K.; Liu, X. Y.; Wen, Z. S. *Electrochem. Solid-State Lett.* **2003**, *6*, A154.
12. Saint, J.; Morcrette, M.; Larcher, D.; Laffont, L.; Beattie, S.; Pérès, J.-P.; Talaga, D.; Couzi, M.; Tarascon, J.-M. *Adv. Funct. Mater*. **2007**, *17*, 1765.
13. Esmanski, A.; Ozin, G. A. *Adv. Funct. Mater*. **2009**, *19*, 1999.
14. Kim, H.; Han, B.; Choo, J.; Cho, J. *Angew. Chem. Int. Ed*. **2008**, *120*, 10305.
15. Hochgatterer, N. S.; Schweiger, M. R.; Koller, S.; Raimann, P. R.; Wöhrle, T.; Wurm, C.; Winter, M. *Electrochem. Solid-State Lett*. **2008**, *11*, A76.
16. Song, S.-W.; Baek, S.-W. *Electrochem. Solid-State Lett*. **2009**, *12*, A23.
17. Zhuang, G. V.; Ross, P. N., Jr. *Electrochem. Solid-State Lett.* **2003**, *6*, A136.
18. Ryu, Y.-G.; Lee, S.; Mah, S.; Lee, D. J.; Kwon, K.; Hwang, S.; Doo, S. *J. Electrochem. Soc*. **2008**, *155*, A583.
19. Choi, N. S.; Yew, K. H.; Lee, K. Y.; Sung, M.; Kim, H.; Kim, S.-S. *J. Power Sources* **2006**, *161*, 1254.
20. Ulman, A. *Chem. Rev*. **1996**, *96*, 1533.
21. Striebel, K. A.; Deng, C. Z.; Wen, S. J.; Cairns, E. J. *J. Electrochem. Soc.* **1996**, *143*, 1821.
22. Song, S.-W.; Reade, R. P.; Cairns, E. J.; Vaughey, J. T.; Thackeray, M. M.; Striebel, K. A. *J. Electrochem. Soc*. **2004**, *151*, A1012.
23. Baek, S.-W.; Hong, S.-J.; Kim, D.-W.; Song, S.-W. *J. Power Sources* **2009**, *189*, 660.
24. Song, S.-W.; Baek, S.-W. *Electrochim. Acta* **2009**, *54*, 1312.
25. Zhuang, G. V.; Xu, K.; Yang, H.; Jow, T. R.; Ross, P. N., Jr. *J. Phys. Chem. B* **2005**, *109*, 17567.
26. Compton, S. V.; Compton, D. A. C. In *Practical Sampling Techniques for Infrared Analysis*; Coleman, P. B., Ed.; CRC Press: Boca Raton, FL, 1993.
27. Han, D.; Lorentzen, J. D.; Weinberg-Wolf, J.; McNeil, L. E. *J. Appl. Phys*. **2003**, *94*, 2930.
28. Brodsky, M. H.; Cardona, M.; Cuomo, J. *Phys. Rev. B* **1977**, *16*, 3556.
29. Baranchugov, V.; Markevich, E.; Pollak, E.; Salitra, G.; Aurbach, D. *Electrochem. Commun*. **2007**, *9*, 796.
30. Tuinstra, F.; Koenig, J. L. *J. Chem. Phys*. **1970**, *53*, 1126.
31. Colthup, N. B.; Daly, L. H.; Wiberley, S. E. *Introduction to Infrared and Raman Spectroscopy*; Academic Press: New York, 1990.
32. Socrates, G. *Infrared Characteristic Group Frequencies, Tables and Charts*; John Wiley & Sons: New York, 1994.
33. Spectral database for organic compounds SDBS, http://riodb01.ibase.aist.go.jp/sdbs
34. Zhang, X.; Kostecki, R.; Richardson, T. J.; Pugh, J. K.; Ross, P. N., Jr. *J. Electrochem. Soc*. **2001**, *148*, A1341.
35. Xu, K. *Chem. Rev*. **2004**, *104*, 4303.
36. Aurbach, D.; Markovsky, B.; Shechter, A.; Ein-Eli, Y. *J. Electrochem. Soc*. **1996**, *143*, 3809.
37. Limthongkul, P.; Jang, Y.-I.; Dudney, N. J.; Chiang, Y.-M. *Acta Materialia* **2003**, *51*, 1103.
38. Schroeder, G.; Gierczyk, B.; Waszak, D.; Walkowiak, M. *Electrochem. Commun*. **2006**, *8*, 1583.
39. Santner, H. J.; Korepp, C.; Winter, M.; Besenhard, J. O.; Moller, K.-C. *Anal. Bioanal. Chem*. **2004**, *379*, 266.
40. Aurbach, D.; Moshkovich, M.; Cohen, Y.; Schechter, A. *Langmuir* **1999**, *15*, 2947.
41. Matsuta, S.; Asada, T.; Kitaura, K. *J. Electrochem. Soc*. **2000**, *147*, 1695.
42. Zhuang, G. V.; Yang, H.; Blizanac, B.; Ross, P. N., Jr. *Electrochem. Solid-State Lett*. **2005**, *8*, A441.
43. Yang, H.; Zhuang, G. V.; Ross, P. N., Jr. *J. Power Sources* **2006**, *161*, 573.